Original Research

L-band radiometers can be used to remotely monitor the microwave brightness temperature of land surfaces. We investigated how soil hydraulic properties and soil moisture contents of a bare soil plot can be inferred from L-band brightness temperatures using a coupled inversion approach.

M. Dimitrov, J. Vanderborght, K.Z. Jadoon, L. Weihermüller, and H. Vereecken, Research Centre Jülich, Institute of Bio- and Geosciences: Agrosphere (IBG 3), Jülich 52425, Germany; K.G. Kostov, Bulgarian Academy of Sciences, Institute of Electronics, Sofia 1784, Bulgaria; K.Z. Jadoon, Water Desalination and Reuse Center, King Abdullah Univ. of Science and Technology, Thuwal 23955-6900, Saudi Arabia; T.J. Jackson and R. Bindlish, USDA-ARS, Hydrology and Remote Sensing Lab., Beltsville, MD 20705-2350; Y. Pachepsky, USDA-ARS, Environmental Microbial and Food Safety Lab., Beltsville, MD 20705-2350; and M. Schwank, Swiss Federal Institute WSL, Mountain Hydrology and Torrents, Zürcherstrasse 111, 8903 Birmensdorf, Switzerland, and Gamma Remote Sensing AG, Worbstrasse 225, 3073 Gümligen, Switzerland. *Corresponding author (j.vanderborght@fz-juelich.de)l

Vadose Zone J.
doi:10.2136/vzj2013.04.0075
Received 23 Apr. 2013.

Soil Hydraulic Parameters and Surface Soil Moisture of a Tilled Bare Soil Plot Inversely Derived from L-Band Brightness Temperatures

M. Dimitrov, J. Vanderborght,* K. G. Kostov, K. Z. Jadoon, L. Weihermüller, T. J. Jackson, R. Bindlish, Y. Pachepsky, M. Schwank, and H. Vereecken

We coupled a radiative transfer model and a soil hydrologic model (HYDRUS 1D) with an optimization routine to derive soil hydraulic parameters, surface roughness, and soil moisture of a tilled bare soil plot using measured brightness temperatures at 1.4 GHz (L-band), rainfall, and potential soil evaporation. The robustness of the approach was evaluated using five 28-d data sets representing different meteorological conditions. We considered two soil hydraulic property models: the unimodal Mualem–van Genuchten and the bimodal model of Durner. Microwave radiative transfer was modeled by three different approaches: the Fresnel equation with depth-averaged dielectric permittivity of either 2- or 5-cm-thick surface layers and a coherent radiative transfer model (CRTM) that accounts for vertical gradients in dielectric permittivity. Brightness temperatures simulated by the CRTM and the 2-cm-layer Fresnel model fitted well to the measured ones. L-band brightness temperatures are therefore related to the dielectric permittivity and soil moisture in a 2-cm-thick surface layer. The surface roughness parameter that was derived from brightness temperatures using inverse modeling was similar to direct estimates from laser profiler measurements. The laboratory-derived water retention curve was bimodal and could be retrieved consistently for the different periods from brightness temperatures using inverse modeling. A unimodal soil hydraulic property function underestimated the hydraulic conductivity near saturation. Surface soil moisture contents simulated using retrieved soil hydraulic parameters were compared with in situ measurements. Depth-specific calibration relations were essential to derive soil moisture from near-surface installed sensors.

Abbreviations: CRTM, coherent radiative transfer model; DBM, Durner bimodal model; DOY, Day of the Year; MvG, Mualem–van Genuchten; RMSD, root mean square deviation.

Knowledge about soil moisture and soil hydraulic properties is essential for weather and climate predictions, as well as to calculate the soil water balance and to determine plant growth and watershed runoff (e.g., Robinson et al., 2008; Vereecken et al., 2008).

Passive microwave remote sensing in the L-band (1–2 GHz) allows the retrieval of soil moisture from the soil brightness temperature (e.g., Shutko, 1982; Schmugge, 1985; Jackson et al., 1999). For more than three decades, various measurement campaigns for the estimation of soil moisture from brightness temperatures using ground- or aircraft-based radiometers have been performed (e.g., de Rosnay et al., 2006; Bindlish et al., 2008; Jonard et al., 2011; Schwank et al., 2012; Montzka et al., 2012). The satellite of the European Space Agency with its Soil Moisture and Salinity Mission (SMOS), which was launched successfully in 2009, and the NASA satellite with its Soil Moisture Active Passive Mission (SMAP), which is scheduled for launch in 2014 to 2015, are equipped, among other measurement systems, with L-band radiometers for measuring brightness temperature (e.g., Kerr et al., 2010; Entekhabi et al., 2010).

The data products can improve meteorological and climate predictions on a global scale (Kerr et al., 2010). On a smaller spatial scale, brightness temperatures measured using ground-based radiometers can provide information about the local surface soil moisture. This information is indispensable for the development of soil moisture retrieval models and the validation of corresponding space-borne data products.

To simulate water and energy fluxes, the soil hydraulic properties, i.e., the soil water retention curve and the hydraulic conductivity curve, which relate volumetric water content, water potential, and hydraulic conductivity, are crucial (Camillo et al., 1986). Soil hydraulic properties are commonly measured in small soil samples. To simulate soil water fluxes at larger scales, spatial distributions of soil hydraulic parameters are derived from soil maps and databases using the relationships between soil hydraulic parameters and soil properties, e.g., soil texture. However, soil hydraulic parameters are known to be highly spatially variable and the question of whether soil properties measured at a small spatial scale can be used to predict time series of averaged fluxes and water contents at a larger spatial scale is the topic of intensive research (Vereecken et al., 2007). To tackle this mismatch between simulation and measurement scales, experimental methods that provide information about soil water content at a larger spatial scale, such as L-band radiometry, are of interest. This larger scale information on soil moisture could be used to derive with inverse modeling the soil hydraulic parameters that are relevant at this scale.

The L-band brightness temperature is, however, not a direct measure of soil moisture. It depends on the vertical distributions of dielectric permittivity and soil temperature and on soil surface roughness (Mattikalli et al., 1998). The dielectric permittivity depends strongly on the soil moisture content and is also influenced by other soil properties such as the bulk density, organic matter, and clay content (e.g., Wang and Schmugge, 1980; Roth et al., 1990). To link the L-band brightness measurements to soil moisture contents, a coupled modeling approach that combines simulations of water, temperature, and dielectric permittivity profiles with simulations of brightness temperatures for a certain soil surface roughness seems necessary. The simulated soil moisture profiles depend on the meteorological boundary conditions (precipitation and soil evaporation) and the soil hydraulic properties. As a consequence, soil hydraulic properties may be retrieved from L-band brightness temperatures using coupled inverse modeling approaches in which models that simulate water and energy fluxes in the soil profile are coupled with dielectric mixing and radiative transfer models (e.g., Mattikalli et al., 1995, 1998; Camillo et al., 1986; Burke et al., 1998; Chang and Islam, 2000).

However, different radiative transfer and hydraulic property models can be used in the coupled inversion, and the parameterization of the soil hydraulic functions as well as the prediction of the soil moisture contents may depend on the chosen models. Therefore, a validation of the derived surface soil moisture contents is necessary. For such a validation, in situ installed soil moisture sensors need to be used. Such sensors always average soil moisture contents throughout a certain soil volume or a certain soil layer thickness. Especially for near-surface measurements of soil moisture, the measurement volume of an in situ sensor may extend into regions above the soil, which affects the sensor reading. Furthermore, the microwave emission depth increases with decreasing moisture (Escorihuela et al., 2010). Both instances make the validation of near-surface soil moisture content retrieved from L-band brightness temperatures using in situ soil moisture probes a nontrivial task.

In this study, we evaluated the effect of using different hydraulic property functions—the unimodal Mualem–van Genuchten model (MvG) (van Genuchten, 1980) vs. the Durner bimodal model (DBM) (Durner, 1994; Priesack and Durner, 2006)—and of using different radiative transfer models—a coherent radiative transfer model (CRTM) that accounts for the effects of vertical gradients of dielectric permittivity close to the soil surface and the Fresnel equation, which assumes a vertically homogeneous dielectric permittivity in the soil profile—on the retrieved soil moisture contents and soil hydraulic parameters. The retrieved soil moisture contents were compared with in situ monitored soil moisture contents. Unlike the other studies presented above, which focused on relatively short measurement periods over undisturbed plots, in this study we considered five 28-d time series consisting of several infiltration, redistribution, and evaporation events to cover a wide range of soil hydrologic conditions. For each time period, an independent set of inversely estimated hydraulic parameters was derived. Variation in the estimated hydraulic parameters between different time periods could be due to changing hydraulic properties of the topsoil layer with time due to, e.g., slacking and compaction. It could also be due to a lack of sensitivity of the L-Band brightness temperatures to a parameter so that this parameter cannot be estimated accurately from brightness temperatures using inverse modeling. By comparing the soil hydraulic properties obtained for the different measurement periods, the robustness of the parameters obtained by the inversion procedure was evaluated.

In addition, we monitored brightness temperatures of the relatively rough surface of a tilled soil. This adds additional complexity because an additional parameter, which needs to be estimated using the inversion routine, has to be included in the model to describe the microwave emission from a rough soil surface.

Materials and Methods

Experimental Setup and Instrumentation

From September 2009 to December 2009 and from March 2011 to September 2011, a trapezoidal bare soil plot with widths between 12 and 8 m and 20-m length was monitored after tilling using a

Fig. 1. The L-band radiometer JÜLBARA and laser profiler over the plot (left); mechanical field preparation (right).

spring tine cultivator (Fig. 1). The plot was located within the Selhausen test site of the Forschungszentrum Jülich, Germany, which is part of the TERENO observatory (Zacharias et al., 2011). The mechanical field preparation was repeated four times during the measurement campaigns: on 27 Sept. 2009 (Day of the Year [DOY] 270), 15 Mar. 2011 (DOY 74), 27 May 2011 (DOY 147), and 11 Aug. 2011 (DOY 223). The field was kept free of weeds using herbicides. The soil has a silt loam texture (14.5% sand, 69% silt, and 16.5% clay) according to the USDA textural classification. A detailed description of the Selhausen test site was given by Weihermüller et al. (2007).

Ten ECH$_2$O 5TE sensors (Decagon Devices) were installed horizontally in five different locations at two different depths: 2 and 5 cm (five sensors per depth). The relative dielectric permittivity of the soil, ε_r, and the soil temperature, T_{Soil} (°C), were recorded in 10-min intervals and stored automatically by two EM50 dataloggers (Decagon Devices).

The Dicke-type L-band radiometer JÜLBARA (operation frequency of 1.4 GHz, equivalent to a wavelength of 21.4 cm) with dual-mode horn antenna (12° full beam width at −3 dB, Schwank et al., 2010b) was mounted on a fixed tower at 12.5-m height above the tilled plot to measure the brightness temperature, TB (K), with fixed angle of incidence $\beta_0 = 50°$ (accounting for a 2° slope of the field plot). The JÜLBARA radiometer was developed as a successor to the ELBARA radiometer (Mätzler et al., 2003) and measures in the protected L-band at two frequency ranges (1.400–1.414 and 1.414–1.427 GHz) simultaneously. The radiometer was equipped with two internal calibration sources: hot load (338 K) and cold load (278 K). Additionally, external calibration of the radiometer with sky measurements was performed daily during the whole investigation period in 2011 and periodically in 2009. The integration time of the measurements was set to 10 s and the sensitivity of the radiometer was 0.1 K. The measurements were recorded continuously in 2-min intervals, but hourly mean values of the measured TB were used in the calculations.

Two weather stations, located on the test site, were used to provide meteorological data during the whole investigation period. The measured air temperature, precipitation, wind speed, humidity at 2-m height. and solar and global radiation were used as forcing for the hydrologic model. From the measured meteorological data, hourly potential evaporation was derived according to FAO guidelines (Allen et al., 1998).

Models

Hydrologic Model

In this study, one-dimensional vertical water flow was simulated in a homogeneous and isotropic rigid porous medium by the Richards equation (Jury et al., 1996):

$$\frac{\partial\theta(h)}{\partial t}=\frac{\partial}{\partial z}\left[K(\theta)\left(\frac{\partial h}{\partial z}+1\right)\right] \qquad [1]$$

where h (cm) is the pressure head, θ (cm^3 cm^{-3}) is the volumetric water content, $K(\theta)$ (cm min^{-1}) is the hydraulic conductivity function, and z (cm) is the elevation (positive upward).

We used either a unimodal or a bimodal pore size distribution model to describe the unsaturated soil hydraulic properties $\theta(h)$ and $K(\theta)$ in Eq. [1]. Both models use the statistical pore-connection model of Mualem (1976) to derive $K(\theta)$ from the $\theta(h)$ functions and use a functional form that was proposed by van Genuchten (1980) to represent pore size distributions. The $\theta(h)$ and $K(\theta)$ functions can be represented in general as (Priesack and Durner, 2006)

$$\theta(h)=\begin{cases}\theta_r+(\theta_s-\theta_r)\left[w_1S_{e1}(h)+w_2S_{e2}(h)\right] & h<0\\ \theta_s & h\geq 0\end{cases} \qquad [2]$$

$$S_{e,i}(h)=\left[1+\left(\alpha_i|h|\right)^{n_i}\right]^{-m_i} \quad [3]$$

$$K(\theta)=K_s\left(w_1S_{e_1}+w_2S_{e_2}\right)^{l} \times\frac{\left\{w_1\alpha_1\left[1-\left(1-S_{e_1}^{1/m_1}\right)^{m_1}\right]+w_2\alpha_2\left[1-\left(1-S_{e_2}^{1/m_2}\right)^{m_2}\right]\right\}^2}{\left(w_1\alpha_1+w_2\alpha_2\right)^2} \quad [4]$$

where θ_r and θ_s are the residual and saturated volumetric water contents ($cm^3\ cm^{-3}$), respectively, S_{ei} is the saturation degree of the ith pore size distribution, α_i (cm^{-1}) and n_i are shape parameters, $m_i = 1 - 1/n_i$, w_i is the volume fraction of the ith pore size distribution with $w_1 + w_2 = 1$, and l is the pore-connectivity parameter, which was assumed to be 0.5 (Mualem, 1976). For $w_2 = 0$, the pore size distribution is unimodal and the MvG functions are obtained (van Genuchten, 1980). For $w_2 > 0$, the pore size distribution is bimodal and the DBM functions (Durner, 1994) are obtained.

The Richards equation was solved numerically using the HYDRUS 1D code (Šimůnek et al., 2008) for a 200-cm-deep soil profile using a spatial discretization of 0.25 cm. Atmospheric boundary conditions using hourly measured rain, calculated potential evapotranspiration rates, and a unit hydraulic head gradient were defined at the top and bottom of the soil profile, respectively. As proposed by Chanzy et al. (2008) for a wet climate, a uniform initial pressure head of −100 cm and a spin-up period of 28 d were used.

Radiative Transfer Model

The microwave brightness temperature of a soil medium, TB, is governed by the dielectric and temperature depth profiles. Brightness temperatures at horizontal polarization, TBH, were used because they are more sensitive to soil moisture changes. Using radiative transfer theory, TBH is given by (Ulaby et al., 1986)

$$\mathrm{TBH}=(1-R_H)T_{eff}+\mathrm{TB}_{sky}R_H \quad [5]$$

where R_H is the reflectivity for horizontal polarization, TB_{sky} is the sky brightness temperature, which was calculated as in Pellarin et al. (2003), and T_{eff} is an effective soil temperature, which can be calculated as shown in Ulaby et al. (1986) if soil moisture and soil temperature profiles are available. Several models were proposed for simplifying the calculation of T_{eff} using limited profile information (Choudhury et al., 1982; Wigneron et al., 2001; Holmes et al., 2006). These models required the so-called deep soil temperature, T_{deep}, measured at least 50 cm below the soil surface. Wigneron et al. (2008) investigated also the simplest possible approximation $T_{eff} \approx T_s(z)$ for z in the range from 0 to 10 cm and found that reasonably good results were obtained for z in the range from 2 to 5 cm. We used the measured soil temperature at 2 cm as an approximation to T_{eff} because, first, we did not have experimental data for the deep soil temperature T_{deep}, and second, the measured temperature T_s (2 cm) characterizes well the temperature variations of the soil layer (0–2 cm) whose thickness is close to the so-called soil moisture sampling depth (Escorihuela et al., 2010; Kostov and Vichev, 1995).

In general, for simulation of soil reflectivity, R_H, the radiative transfer theory differentiates between coherent and noncoherent model approaches, which consider or do not consider, respectively, the phase of the signal (Ulaby et al., 1981). Furthermore, the soil can be considered to be either a dielectrically layered or a homogeneous medium. In this study, we investigated the applicability of a CRTM that resolves the vertical gradients of dielectric permittivity due to gradients in soil moisture content and of the Fresnel equation that assumes a vertically uniform dielectric permittivity or water content in a surface soil layer.

Coherent Radiative Transfer Model

When electromagnetic radiation falls onto a stack of thin films, multiple reflections take place within this structure. Depending on the source of radiation and the layer thickness, the reflected beams may be coherent and interfere with each other (Bass et al., 1995). Figure 2 shows a thin-film system with N layers, where $p_i = \sqrt{(\varepsilon_{r,i})}$ ($\varepsilon_{r,i}$ is the relative dielectric permittivity of the ith soil layer) is the refractive index, d_i is the thickness of the ith layer, and p_s and p_a are the refractive indices of the deeper soil or substrate and the air, respectively. The angle of incidence β_0, the frequency, f, and the polarization of the incident radiation are given as external variables of the system (Bass et al., 1995). The reflection coefficient r_H for horizontal polarization, which is related to the reflectivity R_H as

$$R_H=|r_H|^2 \quad [6]$$

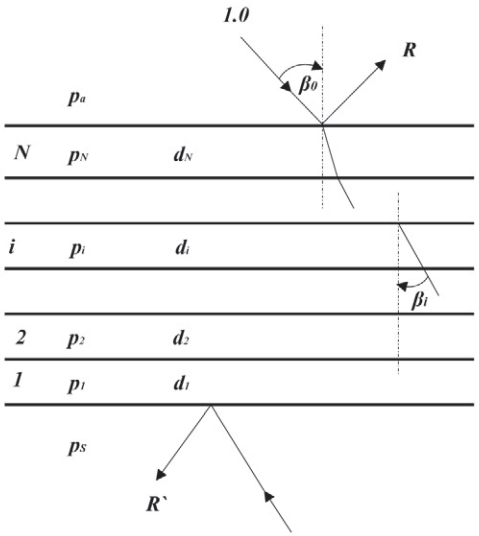

Fig. 2. Parameters of the multilayer coherent radiative transfer model (from Bass et al., 1995).

is, for the multilayer with N layers given by (Bass et al., 1995),

$$r_H = \frac{\eta_a \mathbf{e}_a - \mathbf{h}_a}{\eta_a \mathbf{e}_a + \mathbf{h}_a} \quad [7]$$

where η_a is effective refractive index of air and $\mathbf{e}_a$ and $\mathbf{h}_a$ are electric and magnetic vectors in the incident medium (air). The effective refractive index of the soil medium or substrate is given by

$$\eta_x = \frac{p_x}{\cos\beta_x} \quad [8]$$

where β_x is the incidence angle in a layer or in the substrate, which is related by Snell's law to the refractive index of the air and incidence angle β_0 as

$$p_a \sin\beta_o = p_x \sin\beta_x \quad [9]$$

The vectors $\mathbf{e}_a$ and $\mathbf{h}_a$ are given by

$$\begin{bmatrix} \mathbf{e}_a \\ \mathbf{h}_a \end{bmatrix} = \mathbf{M} \begin{bmatrix} 1 \\ \eta_s \end{bmatrix} \quad [10]$$

where $\mathbf{M}$ is the product matrix given by

$$\mathbf{M} = M_N M_{N-1} \ldots \mathbf{M}_i \ldots M_2 M_1 \quad [11]$$

where $\mathbf{M}_i$ is a 2×2 matrix and represents the ith layer of the system:

$$\mathbf{M}_i = \begin{bmatrix} \cos\partial_i & \frac{j}{\eta_i}\sin\partial_i \\ j\eta_i \sin\partial_i & \cos\partial_i \end{bmatrix} \quad [12]$$

where j is the imaginary number, $\partial_i = 2\pi/\lambda(p_i d_i \cos\beta_i)$, and λ is the wavelength.

The considered layer thickness corresponded with the spatial discretization used for the soil water flow simulations using HYDRUS 1D and was 0.25 cm, which corresponds with approximately 1% of the L-band wavelength in free space. In general, the layer thickness must be much smaller than the wavelength to obtain accurate results. The layer thickness of 0.25 cm was selected as a compromise between the model calculation time and accuracy.

From the simulated θ profiles, ε_r depth profiles were calculated using the dielectric mixing model (Wang and Schmugge, 1980).

Fresnel Equation

For a soil with a smooth surface and constant dielectric properties with depth, the reflectivity R_H can be calculated using the Fresnel equation (e.g., Njoku and Entekhabi, 1996):

$$R_H = \left(\frac{\cos\beta_0 - \sqrt{\varepsilon_r - \sin^2\beta_0}}{\cos\beta_0 + \sqrt{\varepsilon_r - \sin^2\beta_0}} \right)^2 \quad [13]$$

The relative dielectric permittivity ε_r in the Fresnel equation was obtained by taking the arithmetic mean of the relative dielectric permittivities in the 2- and 5-cm topsoil layers, which were derived from HYDRUS 1D simulated θ profiles using the dielectric mixing model of Wang and Schmugge (1980). These layers were selected because good correspondence between L-band brightness temperatures and soil moisture was observed experimentally for soil layer depths between 2 and 5 cm (e.g., Newton et al., 1982; Wang, 1987; Kostov and Vichev, 1995; Jackson et al., 1997). In the following, we use Fresnel 0–5 cm and Fresnel 0–2 cm to indicate that TBH values were calculated using the Fresnel equation (Eq. [13]) with averaged relative dielectric permittivities, ε_r, in the 0- to 5 and 0- to 2-cm surface soil layers, respectively.

Surface Roughness Correction Model

For a rough soil surface, Eq. [6] and [13] for calculating the soil reflectivity must be modified to account for surface scattering. As the surface roughness increases, the brightness temperature increases and the sensitivity of the brightness temperature to soil moisture decreases (Njoku and Entekhabi, 1996). Random rough surfaces are typically characterized in physically based radiative transfer models using statistical parameters, such as the standard deviation of surface heights or the root mean square roughness height, σ, the spatial correlation length, and a spatial correlation function (Ulaby et al., 1982; Fung, 1994; Schwank et al., 2010a). These physically based models provide insight into the scattering mechanisms but are often computationally intensive and require detailed information about the surface roughness. For this reason, simpler semi-empirical roughness correction models have often been used in retrieval and inversion algorithms.

For correcting the roughness effects, we used a simpler model that was proposed by Choudhury et al. (1979) and considers only the root mean square roughness height, σ. According to this model, the rough surface reflectivity, R_{rH}, is related to the reflectivity of a smooth surface, R_H, as

$$R_{rH} = R_H \exp\left(-\frac{16\pi^2}{\lambda^2}\sigma^2 \cos^2\beta_0 \right) \quad [14]$$

This model was verified using radiometric measurements (Ulaby et al., 1986), and it was shown that σ values retrieved from brightness temperatures using Eq. [14] were smaller than the measured ones. Recently, Wigneron et al. (2011) showed that σ that was estimated from L-band radiometric measurements using Eq. [14] underestimates the root mean square roughness height derived from direct measurements. Therefore, σ in Eq. [14] was considered as an additional fitting parameter. It should be noted that this model does not consider the effects of larger scale (regular) structures, e.g., periodic structures with a scale larger than approximately 0.1 m, that cannot be treated as random roughness (Schwank et al., 2010a) and that might be expected in moldboard-tilled fields. In chisel-tilled fields, however, such regular structures are less pronounced

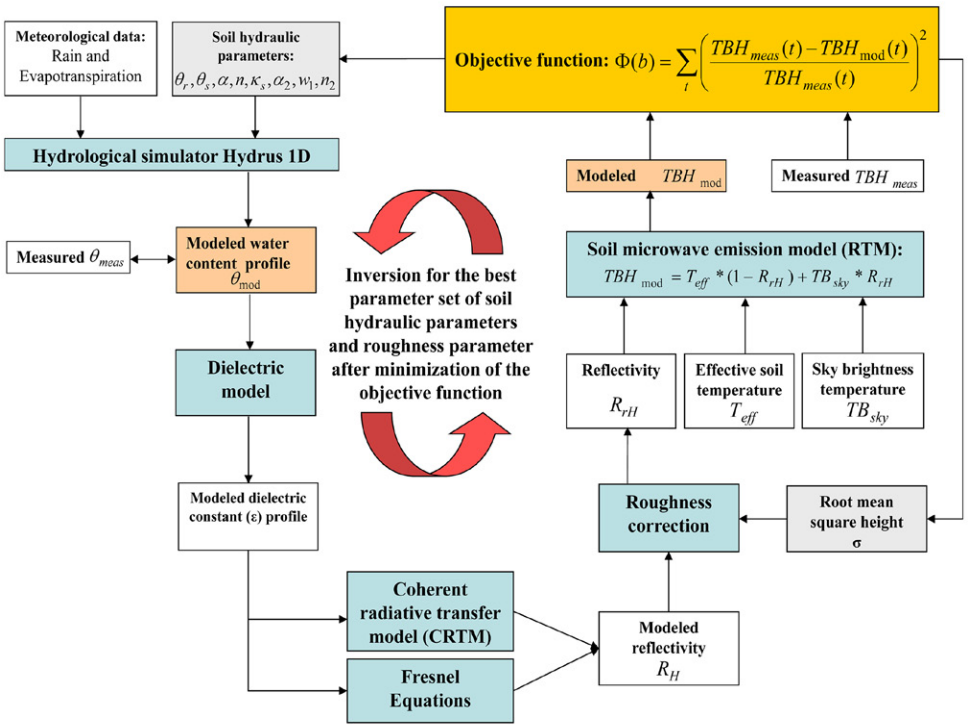

Fig. 3. Flow chart of the coupled inversion procedure. Blue-filled boxes represent models, white boxes are input or output variables, gray-filled boxes are model parameters that are derived from minimizing the objective function (gold-filled box), orange-filled boxes are output variables that are compared with measurements.

so that Eq. [14] was used to model the effect of surface roughness in this study.

Model Coupling and Parameter Estimation

The models described above were coupled as shown in Fig. 3. The HYDRUS 1D code was used to generate soil moisture profiles. Dielectric permittivity profiles $\varepsilon_r(z)$ were calculated from these soil moisture profiles using the dielectric model of Wang and Schmugge (1980). In the next step, R_H was calculated from these $\varepsilon_r(z)$ profiles with the CRTM or the Fresnel model and corrected for surface roughness using Eq. [14]. Finally, brightness temperatures, TBH, were calculated using Eq. [5]. The models with their inputs and outputs are presented in Table 1.

In the optimization procedure, the objective function, i.e., the sum of the squared normalized differences between measured and modeled brightness temperatures, was minimized by fitting the hydraulic soil parameters of the topsoil layer (0–30 cm) and the root mean square roughness height, σ. A global optimization approach, the Shuffled Complex Evolution (SCE-UA) (Duan et al., 1993) was used to derive the optimal parameter set that minimizes the objective function. When the objective function did not decrease by >0.001% after 20 successive parameter updates, the inversion was stopped. Similar stopping criteria for the SCE-UA algorithm were used in other coupled inversion routines that derived soil hydraulic properties from off-ground radar measurements (e.g., Jadoon et al., 2012; Lambot et al., 2009).

The data series was split up into five 28-d periods (DOY 272–300, 2009; DOY 92–120, 2011; DOY 158–186, 2011; DOY 188–216, 2011; and DOY 226–254, 2011). For each of these periods, the soil hydraulic parameters and root mean square roughness height were optimized using the above-described inversion approach. By splitting up the data set, the inversion approach could be tested for different soil hydrologic conditions. Some meteorological and measured parameters for all of the periods are summarized in Table 2. In general, the periods may be characterized as mostly dry with a maximum brightness temperature of 279.6 K (DOY 92–120, 2011), mostly wet with a minimum brightness temperature of 138.5 K (DOY 226–254, 2011, and DOY 188–216, 2011), or mixed (with dry and wet phases). The total amount of rain ranged between 1.49 cm (DOY 92–120, 2011) and 19.74 cm (DOY 158–186, 2011). The different amounts of rainfall in the different periods were reflected in large variations in surface soil moisture contents. Field preparation was done between some of these periods, which changed the surface roughness, and the soil moisture sensors were reinstalled.

In the following, we focused on two time series that differed strongly: a dry period (DOY 92–120, 2011) and a wet period (DOY 158–186, 2011). Data for the other periods are given in the

Table 1. Inputs and outputs of the coupled inversion scheme.

Model	Input	Output
Hydrologic model	rain and ETo	soil moisture profile
Dielectric model	soil moisture profile	relative dielectric permittivity [$\varepsilon_r(z)$]
Coherent radiative transfer model or Fresnel equation	$\varepsilon_r(z)$	reflectivity (R_H)
Roughness correction	R_H and roughness coefficient (σ^2)	roughness corrected reflectivity (R_{rH})
Radiative transfer model	R_{rH} and effective temperature (T_{eff})	brightness temperature (TBH)

Table 2. Ranges of air temperature (T_{air}), L-band brightness temperature for horizontal polarization (TBH), volumetric soil moisture (θ), and cumulative rainfall during the different observation periods.

Day of the Year	Parameter	T_{air}	TBH	θ at 2 cm	θ at 5 cm	Total rainfall
		K		$cm^3\ cm^{-3}$		cm
92–120, 2011	min.	275.9	205.14	0.087	0.12	1.49
	max.	300.6	279.58	0.184	0.195	
	difference	24.7	74.44	0.097	0.075	
158–186, 2011	min.	281.6	146.5	0.218	0.206	19.74
	max.	306.8	232.4	0.362	0.347	
	difference	25.2	85.9	0.144	0.141	
188–216, 2011	min.	281.8	138.54	0.178	0.175	6.61
	max.	302.3	263.9	0.315	0.286	
	difference	20.5	125.36	0.137	0.111	
226–254, 2011	min.	281.4	139.48	0.255	0.221	9.01
	max.	306.3	250.6	0.391	0.369	
	difference	24.9	111.12	0.137	0.149	
272–300, 2009	min.	275.1	165.58	0.163	0.185	5.7
	max.	293.16	251.2	0.326	0.335	
	difference	18.06	85.62	0.163	0.15	

supplementary material to demonstrate that similar results were obtained for those periods.

Model Validation

To validate the inversely derived or retrieved soil hydraulic properties from L-band brightness temperatures, they were compared with hydraulic properties determined on soil samples in the laboratory. Five cylindrical undisturbed soil samples of 100 cm^3 (5.1-cm length and 5-cm i.d.) were taken from the topsoil layer (0–5-cm depth) on DOY 80, 2011. The soil water retention curve was obtained by equilibrating the samples at different pressure heads after placing them on a sand box with a hanging water table or in pressure cells. The saturated hydraulic conductivity was measured with a permeameter using the constant-head method.

The water contents measured by 5TE sensors installed at the 2- and 5-cm depths were compared with water contents at these depths simulated by HYDRUS 1D using the optimized hydraulic properties. Because a soil moisture sensor does not measure at a single depth but averages water contents within a certain volume of influence, differences between the simulated water contents at the sensor depth and the water contents actually measured by the sensor can be expected. A detailed analysis and an exact evaluation of the sensor's volume of influence and the distribution of weighting factors that are used to calculate depth-weighted averaged water contents would require the calculation of electromagnetic fields generated by the sensor in a heterogeneous medium around the sensor, which is beyond the scope of this study. However, to obtain a first rough estimate of the impact that vertical variations of water contents could have on sensor readings and their comparison with simulated water contents at a single depth, we used a very crude approximation, which is outlined below, of the measurement volume of the 5TE sensor and the distributions of weighting factors within it. Subsequently, these weighting factors were used to calculate depth-averaged water contents from simulated water content profiles, which were compared with simulated water contents at the 2- and 5-cm depths. According to the manufacturer, the volume of influence of the 5TE sensors is 0.3 L (Decagon Devices, 2009). As a simple approximation, we assumed that the 0.3-L volume corresponds to a block of 6.5 by 6.5 by 7.2 cm (7.2 cm is an estimate of the radiating length of the sensor) and that the sensor averages the dielectric permittivity within this volume. For the sensor at the 2-cm depth, the measurement volume would also include a 1.25-cm-thick air layer with air dielectric permittivity $\varepsilon_a = 1$. According to the manufacturer of the 5TE sensors, the electromagnetic field produced by the sensor decreases with distance from the sensor electrodes (Decagon Devices, 2009). However, the distribution of the sensor sensitivity to soil dielectric permittivity (water content) within the 0.3-L volume of influence is not known. To mimic the averaging performed by the 5TE sensors, we assumed that the weighting factors used for calculating the depth-weighted mean of simulated soil moisture contents decrease linearly with distance from the sensor electrodes. We also assumed that the weighting factors at the upper and lower surface of the presumed measurement volume are equal to $1/e = 0.3679$ of its value in the center of the measurement volume.

To relate the sensor readings to soil water contents, soil- and depth-specific calibration relations were derived as proposed by the manufacturer (Cobos and Chambers, 2011). By using depth-specific calibration relations, the impact of the air layer on the measurement by the sensor at the 2-cm depth was indirectly accounted for. A box with a surface of 60 by 40 cm and a height of 32 cm was filled with soil taken from the test site. Starting from sieved and air-dried soil ($\theta \sim 0.04\ cm^3\ cm^{-3}$), the soil was wetted to full saturation ($\theta \sim 0.44\ cm^3\ cm^{-3}$) in seven steps. After every step, the soil was again well mixed and homogenized and repacked into the box. For each step, the volumetric water content was determined on at least two 100-cm^3 soil samples. Ten sensors, two at each depth, were installed horizontally in the soil box between 1.8 and 12 cm below the soil surface. The raw sensor readings of the 5TE sensors were transformed into relative dielectric permittivity using ε_r = RawData/50 (Decagon Devices, 2010).

The inversely estimated soil surface roughness parameter σ was compared with the root mean square roughness height that was derived from the three-dimensional laser profiler LMP-II, developed by the Institute of Agricultural Engineering, University of

Bonn, Germany. More information about the measurement system is given in Sun et al. (2006). For each measurement, 124 parallel profiles of 1500-mm length were sampled with a sampling interval of 2 mm. The distance between parallel profiles was 4 mm. The obtained surface heights were detrended using a two-dimensional linear fit and the variance of the detrended surface heights in the scanned plot was determined from the variances, σ_i^2, and means, μ_i, of the detrended surface heights along individual profiles as

$$\sigma^2 = \frac{1}{N}\sum_{i=1}^{N}\sigma_i^2 + \frac{1}{N-1}\sum_{i=1}^{N}(\mu_i - \mu_.)^2 \quad [15]$$

where N is the number of profiles and $\mu_.$ is the average of the detrended surface heights in the plot.

The laser profiler measurements were done at the start of the measurement periods. Due to rainfall, the surface roughness decreased with time. To account for this decrease, we assumed that the root mean square roughness height decreases exponentially with the accumulated amount of rainfall and could be calculated as (Zobeck and Onstand, 1987)

$$\sigma(P) = \sigma 0.89\exp(-0.026P) \quad [16]$$

where $\sigma(P)$ is the root mean square roughness height after a certain amount of cumulative precipitation P (cm).

Results and Discussion

Measured and Modeled Brightness Temperature

The modeled brightness temperatures were derived based on measurements of soil temperature and on simulations of the water content profiles using fitted DBM or MvG parameters in combination with either the CRTM or the Fresnel equation with averaged dielectric permittivity in the 0- to 2- or 0- to 5-cm soil layers.

Figure 4 shows the modeled and measured brightness temperatures at horizontal polarization (TBH) as well as the measured precipitation. During days without rain, diurnal variations in TBH up to 20 K were mainly caused by diurnal variations in soil temperature. Also, diurnal fluctuations in the surface soil water content and dielectric permittivity resulting from diurnal evaporation dynamics contributed to the diurnal TBH dynamics. The measured and simulated diurnal water content fluctuations were small (0.01 cm^3 cm^{-3}), however, so that their effect on TBH was small when compared with the fluctuations in TBH due to soil temperature fluctuations. The comparison between the measured and modeled TBH confirm that for wet soil the diurnal TBH fluctuations can be reproduced well using the approximation $T_{eff} \approx T_s$ (2 cm) (e.g., Fig. 4b and Supplementary Fig. A2). To the contrary, for dry soil (e.g., Fig. 4a, DOY 105–116), the modeled diurnal TBH variations were bigger than the measured ones. This indicates that diurnal variation in the soil temperature at the 2-cm depth is larger than the variation in the effective temperature, which is in agreement with the fact that the effective sampling depth of the radiometer increases when the soil gets drier. Several rain events occurred during the mostly dry period (DOY 92–120), which were immediately observed by the radiometer. The measured TBH decreased by >50 K just after the main rain events and increased again subsequently due to drying out of the soil surface. After the rain events (e.g., DOY 103 and 117), the TBH values modeled with Fresnel 0–5 cm were not able to reach the measured TBH and were considerably different from the modeled TBH using Fresnel 0–2 cm or using the CRTM. On DOY 117, differences of 43 K between the CRTM and Fresnel 0–5 cm, of 26.2 K between the CRTM and Fresnel 0–2 cm, and of 18.8 K between Fresnel 0–2 cm and Fresnel 0–5 cm were obtained. After rain, the upper part of

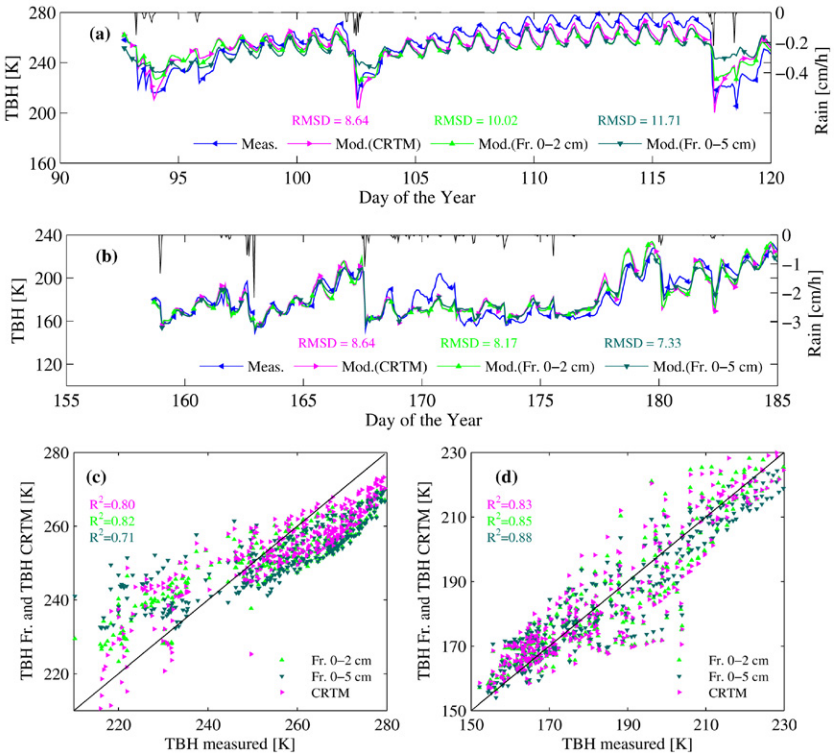

Fig. 4. (a,b) Time series and (c,d) one-to-one plots of measured and modeled brightness temperatures, TBHs, from simulated soil moisture profiles using the Durner bimodal model coupled with the coherent radiative transfer model CRTM or with the Fresnel (Fr.) equation using the mean dielectric permittivity of the 0- to 2- or 0- to 5-cm surface layer for periods (a,c) Day of the Year (DOY) 92 to 120, 2011, and (b,d) DOY 158 to 186, 2011. Black lines in (a) and (b) represent the hourly precipitation rates during the investigated periods.

the soil surface layer was wetted, whereas the deeper part was still dry. This led to different values of the calculated mean dielectric permittivity used in the Fresnel equation (Eq. [13]), depending on the thickness of the surface layer that was considered. During the drying phase after the second rain event (DOY 103), all the models underestimated the TBH. This indicates that the models overestimated the surface soil moisture and hence the dielectric permittivity during this evaporation period.

The total amount of rain during the wet period (DOY 158–186) presented in Fig. 4b was more than a factor 10 larger than during the dry period (see Table 2). During the dry period, the rain events can be characterized as light rain with precipitation rates up to 0.25 cm h^{-1}, whereas during the wet period most of the rain events can be classified as heavy rain with precipitation rates between 1 and 2 cm h^{-1}. The root mean square deviation (RMSD) values between the measured and modeled TBH given in Fig. 5 differed among the periods and the models.

When considering all periods and both hydraulic soil functions (MvG and DBM), the RMSDs varied from 4.4 K for the period DOY 272 to 300, 2009, with DBM and CRTM up to 16.9 K for the period DOY 226 to 254, 2011, with DBM and Fresnel 0–2 cm and 17.7 K with Fresnel 0–5 cm (see Fig. 5a and 5b). In general, RMSDs are fairly similar for the different soil hydraulic functions (DBM and MvG). For two of the wet periods (DOY 158–186, 2011, and DOY 188–216, 2011), the RMSDs were very similar for all model combinations and varied between 8.0 and 8.9 K. During these wet periods, the simulated soil moisture contents were apparently relatively uniform within the surface soil layer so that both the Fresnel 0–2 cm and Fresnel 0–5 cm models, which do not resolve vertical variations of relative dielectric permittivity or soil moisture with depth, gave results similar to the CRTM model. It must be noted that this behavior is closely linked to the hydraulic properties of the fine-textured soil with a relatively large water holding capacity. In a coarse-textured soil, the soil surface layer may rapidly lose a large amount of water and dry out considerably due to rapid drainage so that even during relatively wet periods, large vertical gradients in water content may occur after a rainfall event. For the other periods, the DBM model coupled with the CRTM resulted in the smallest RMSDs. They were comparable with the results from Fresnel 0–2 cm but smaller than the RMSDs obtained with Fresnel 0–5 cm. In these periods, vertical variations in soil moisture and dielectric permittivity in the topsoil layer, e.g., after a rainfall event on a dry soil, that can be accounted for by the CRTM apparently influenced the calculated TBHs. Yet, using a sufficiently shallow surface soil layer for calculating the average dielectric permittivity or moisture content, i.e., Fresnel 0–2 cm, may still be a viable alternative to reproduce the dynamics of measured TBHs. In addition, the DBM model has more flexibility than the MvG model to represent the soil hydraulic properties and consequently simulate the dynamics of the soil moisture contents and match the simulated TBHs to the measured ones.

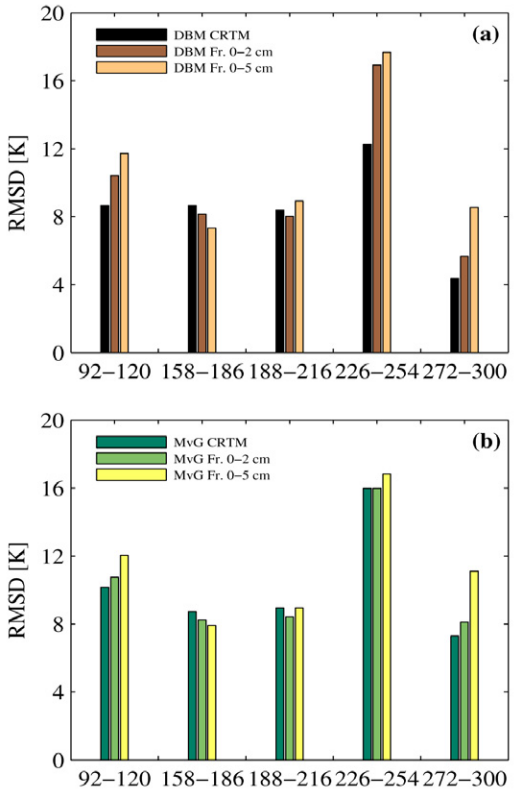

Fig. 5. Root mean square deviations (RMSDs) between measured and modeled L-band brightness temperatures (TBH) for different combinations of radiative transfer models: Fresnel equation (Fr.) or coherent radiative transfer model (CRTM) with soil hydraulic functions: (a) Durner bimodal model (DBM) or (b) Mualem–van Genuchten (MvG).

Surface Roughness Correction Factor

The root mean square roughness height that was derived from laser profiler measurements varied between 1.41 and 2.19 cm for the investigated periods (Table 3). The roughness parameter σ of the model of Choudhury et al. (1979) (Eq. [14]) that was retrieved from the brightness temperatures using inverse modeling did not vary a lot between the different radiative transfer and soil hydraulic property models for a given measurement period and ranged from 1.01 to 2.52 cm (Table 3). Of note is that, except for the dry period DOY 92 to 120, 2011, σ retrieved using Fresnel 0–5 cm was slightly smaller than for the case in which Fresnel 0–2 cm was used. The range of retrieved σ was similar to the range of measured (Eq. [15]) and calculated σ values (Eq. [16]), which represent the roughness at the beginning and the end of the L-band measurement period, respectively. However, the variation in measured σ between different periods was not reproduced by the retrieved values.

The retrieved roughness parameter was larger for the period DOY 92 to 120, 2011, and smaller for the period DOY 158 to 186, 2011, than the measured roughness parameter. It should be noted that for the period DOY 92 to 120, 2011, the retrieved hydraulic functions for the DBM and MvG models also deviated considerably from the other periods and from the laboratory-derived curves (see

Table 3. Dates of mechanical field preparations and laser profiler measurements, root mean square roughness height σ measured with the laser profiler, calculated from the amount of rain since the measurement day until the end of the measurement period, σ(*P*), and inverted from measured brightness temperatures for different measurement periods using the coherent radiative transfer model (CRTM) or the Fresnel equation with depth-averaged dielectric permittivity in the 0- to 2- or 0- to 5-cm surface layer and the Durner bimodal model (DBM) or the Mualem–van Genuchten (MvG) soil hydraulic functions.

Period	Preparation day	Measurement day	σ							
			Measured	σ(P)	Inverted					
					CRTM with DBM	Fresnel 0–2 cm DBM	Fresnel 0–5cm DBM	CRTM with MvG	Fresnel 0–2 cm MvG	Fresnel 0–5 cm MvG
	d of the yr		cm							
92–120	74	96	1.41 (0.97–1.79)†	1.20	2.50	2.38	2.52	2.37	2.35	2.39
158–186	147	158	2.19 (1.97–2.48)	1.37	1.28	1.24	1.19	1.24	1.25	1.13
188–216	147	186	1.60 (1.33–1.86)	1.20	1.65	1.62	1.50	1.59	1.58	1.41
226–254	223	224	1.50 (1.05–1.82)	1.00	1.04	1.08	1.04	1.02	1.02	1.01

† Values in parentheses are the minimal and maximal σ_i along individual profiles.

below and Fig. 6). The difference between the directly measured and inversely estimated roughness parameter σ could be attributed to: (i) the difference between the small 1.5- by 0.5-m footprint of the laser profiler and the much larger footprint of the radiometer combined with the large spatial variability of the surface roughness of tilled soil, as is evidenced by the variability of σ derived from individual profiles (see values in parentheses in Table 3); (ii) the impact of the simultaneous inverse estimation of several parameters, i.e., the hydraulic parameters and σ, which due to multicolinearity may increase the uncertainty of individual parameter estimates; or (iii) temporal variability of the surface roughness with time (due to rain and erosion) vs. constant surface roughness with time in the inversion routine. Finally, it should be noted that the roughness correction model is a semi-empirical model so that the fitted roughness parameter is not necessarily directly comparable with a direct estimation of this parameter from measurements of the soil surface roughness. Despite the problems listed above, however, our results show that plausible estimates of the soil surface roughness parameter σ, i.e., in the same order of magnitude as direct measurements, are obtained when it is estimated together with soil hydraulic parameters from radiometer measurements using a coupled inversion approach. To validate this finding, further studies in which the surface roughness is varied more than in this study have to be performed.

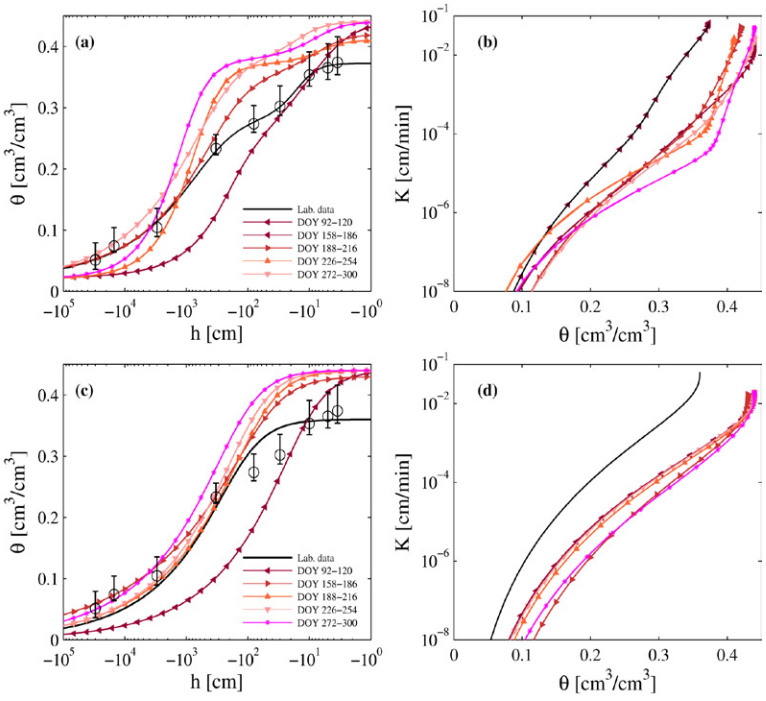

Fig. 6. (a,c) Volumetric water content θ as a function of pressure head, *h*, and (b,d) hydraulic conductivity, *K*, as function of θ for (a,b) the Durner bimodal model and (c,d) the Mualem van Genuchten model. The parameters of the curves were retrieved from time series of the brightness temperatures using the coherent radiative transfer model for different time periods (as Day of the Year, DOY). The black lines represent water retention and conductivity curves that were derived from laboratory measurements; open circles are mean values and the bars represent the ranges. For the hydraulic conductivity curve, only the saturated hydraulic conductivity was measured.

Water Retention and Hydraulic Conductivity Functions

Figure 6 presents water retention (Fig. 6a and 6c) and hydraulic conductivity curves (Fig. 6b and 6d) for the DBM (Fig. 6a and 6b) and the MvG (Fig. 6c and 6d) models that were derived from the measured brightness temperatures for each of the investigated periods using the coupled inversion scheme with the CRTM radiative transfer model. Similar graphs obtained with the Fresnel 0–2 cm layer model are given in the supplementary material (Supplementary Fig. A1). The black open circles (Fig. 6a and 6c) show the mean water contents of five undisturbed

soil samples, and the bars show the maximum and the minimum at each pressure step. The black lines are the water retention curves fitted to the laboratory data. For the hydraulic conductivity curve, the measured saturated conductivity of the soil samples and the Mualem model were used to derive the conductivity curve from the water retention curve. In Tables 4 and 5, the parameters of the DBM and of the MvG hydraulic functions that were derived

Table 4. Parameters of the Durner bimodal soil hydraulic functions derived from laboratory measurements on soil cores and retrieved for the different measurement periods from measured brightness temperatures using coupled inversion with the coherent radiative transfer model (CRTM) or the Fresnel equation with depth-averaged dielectric permittivity in the 0- to 2-cm surface layer. The last two rows show the ranges of inverted parameter values obtained for the different measurement periods.

Model	Period	θ_r	θ_s	α_1	n_1	K_s	λ	w_2	α_2	n_2
	d of the yr	——— $cm^3\ cm^{-3}$ ———		cm^{-1}		$cm\ min^{-1}$			cm^{-1}	
		Laboratory data								
		0.01	0.373	0.0032	1.44	0.066	0.5	0.26	0.0759	2.64
		Inverted from brightness temperatures								
	initial range	0–0.05	0.30–0.45	$(1–100)10^{-3}$	1.1– 2	$(20–200)10^{-3}$	0.5	0.1–0.6	$(10–600)10^{-3}$	1- 4
CRTM	92–120	0.02	0.44	0.0066	1.98	0.020	0.5	0.6	0.22	1.47
Fresnel	92–120	0	0.44	0.0048	1.98	0.020	0.5	0.6	0.33	1.46
CRTM	158–186	0.02	0.42	0.005	1.46	0.054	0.5	0.17	0.2	1.92
Fresnel	158–186	0.01	0.42	0.0051	1.72	0.0513	0.5	0.14	0.34	2.33
CRTM	188–216	0.02	0.41	0.0019	1.98	0.027	0.5	0.1	0.195	2.3
Fresnel	188–216	0.02	0.44	0.0039	1.88	0.027	0.5	0.22	0.16	2.7
CRTM	226–254	0.01	0.44	0.0034	1.43	0.0277	0.5	0.14	0.09	2.12
Fresnel	226–254	0.01	0.43	0.0019	1.43	0.0427	0.5	0.12	0.09	2.06
CRTM	272–300†	0.02	0.44	0.0011	1.99	0.052	0.5	0.15	0.178	1.98
Fresnel	272–300†	0.02	0.43	0.0012	1.99	0.051	0.5	0.12	0.27	1.99
CRTM	range	0.01–0.02	0.41–0.44	0.0011–0.0066	1.43–1.99	0.02–0.054	0.5	0.1–0.6	0.09–0.22	1.47–2.3
Fresnel	range	0–0.02	0.42–0.44	0.0012–0.0051	1.43–1.99	0.02–0.053	0.5	0.12–0.6	0.09–0.34	1.8–2.7

† Data from 2009.

Table 5. Parameters of the Mualem–van Genuchten soil hydraulic functions derived from laboratory measurements on soil cores and retrieved for the different measurement periods from measured brightness temperatures using coupled inversion with the coherent radiative transfer model (CRTM) or the Fresnel equation with depth-averaged dielectric permittivity in the 0- to 2-cm surface layer. The first row shows the ranges of parameter values that were used for the inversion, the last two rows show the ranges of inverted parameter values obtained for the different measurement periods.

Model	Period	θ_r	θ_s	α	n	K_s	λ
	d of the yr	—— $cm^3\ cm^{-3}$ ——		cm^{-1}		$cm\ min^{-1}$	
		Laboratory data					
		0.00	0.36	0.0083	1.44	0.066	0.5
		Inverted from brightness temperatures					
	initial range	0–0.05	0.30 0.45	$(1–100)10^{-3}$	1.1- 2	$(20–200)10^{-3}$	0.5
CRTM	92–120	0.02	0.44	0.091	1.43	0.0204	0.5
Fresnel	92–120	0,02	0.44	0.091	1.42	0.0200	0.5
CRTM	158–186	0.01	0.43	0.02	1.31	0.0204	0.5
Fresnel	158–186	0.02	0.43	0.024	1.33	0.0201	0.5
CRTM	188–216	0.01	0.44	0.0158	1.4	0.0201	0.5
Fresnel	188–216	0.01	0.44	0.04	1.44	0.0201	0.5
CRTM	226–254	0.02	0.44	0.0115	1.42	0.0209	0.5
Fresnel	226–254	0.02	0.44	0.012	1.42	0.0204	0.5
CRTM	272–300†	0.0	0.44	0.0079	1.4	0.0206	0.5
Fresnel	272–300†	0.0	0.44	0.0079	1.38	0.0206	0.5
CRTM	range	0–0.02	0.43–0.44	0.0079–0.091	1.31–1.42	0.0201–0.0209	0.5
Fresnel	range	0–0.02	0.43–0.44	0.0079–0.091	1.33–1.44	0.02–0.0206	0.5

† Data from 2009.

from the laboratory data and from the inversion of the brightness temperatures in the different periods are given.

The laboratory-derived water retention data suggest a bimodal pore size distribution (w_2 is clearly larger than 0 and α_2 is considerably larger than α_1, see Table 4). This behavior could also be observed from the retrieved parameters from inversion of L-band brightness temperatures (Table 4). The variation of the hydraulic parameters and the retrieved retention and conductivity curves, which were obtained from the different time periods, reflects both uncertainty and temporal variation in the hydraulic properties. The different meteorological conditions and consequently different soil hydrologic states during the different periods constrain the hydraulic functions in different ranges of pressure heads, water contents, and conductivities, which also influences the retrieved hydraulic parameters. Especially for the dry period (DOY 92–120, 2011; brown line in Fig. 6), when the soil was drier and pressure heads lower than in the other periods, the derived hydraulic curves for the DBM and MvG models deviate considerably from the other periods and from the laboratory-derived curves. The ranges of the retrieved parameters for the different periods are smaller than the initial parameter ranges that were considered as possible parameter values in the optimization algorithm. This indicates that the L-band brightness temperatures contain information to constrain the hydraulic parameters. The Fresnel and CRTM radiative transfer models give similar ranges of retrieved parameters so that the choice of the radiative transfer model does not have a notable effect on the retrieved parameters.

When comparing the laboratory-derived and retrieved parameters in Tables 4 and 5, there are some differences for the saturated water content, θ_s, saturated conductivity, K_s, the shape parameter, α_2, and the volume fraction, w_2, of the "macropore" domain. The saturated soil moisture values, θ_s, that were retrieved from L-band measurements varied for all periods between θ_s = 0.41 and 0.44 $cm^3\ cm^{-3}$ and were higher than θ_s estimated from the laboratory data (θ_s = 0.373 $cm^3\ cm^{-3}$). The lower estimates obtained from the laboratory data could be explained by the extrapolation of the water retention curve from the point with the highest matric head to the water content for a matric head of 0 cm. The highest pressure head that was considered for the water retention curves was on average −3.5 cm, i.e., the equilibrium pressure head in the middle of the soil sample when the water level was 1 cm below the bottom of the soil sample. At this pressure head, the larger interaggregate pores of the tilled soil were drained already so the saturated water content might be larger than the measured water content at −3.5 cm. A porosity of 0.44 was calculated from the measured dry bulk density of the soil cores (1.49 g cm^{-3}) that is also considerably larger than the measured water content at −3.5 cm but corresponds better with θ_s retrieved from L-band measurements. The fact that water contents in the laboratory samples were not measured for pressure heads larger than −3.5 cm may explain why the α_2 parameter that was derived from the laboratory data was smaller than the α_2 parameter that was retrieved from L-band brightness temperatures. The inverse of α_2 is related to an effective pore size of the macropore region, of which apparently only the smaller pores were filled with water at a pressure head of −3.5 cm in the laboratory samples. In a similar vein, the volume fraction of the macropore domain, w_2, that was derived from brightness temperatures was in most cases larger than the w_2 derived from laboratory measurements.

The retrieved saturated hydraulic conductivity was smaller than the laboratory-measured saturated conductivity, especially for the unimodal MvG model. The saturated conductivity that is measured on 5.1-cm-long soil columns may be very large when large pores that connect the in- and outflow side of the column are present. In the field soil, the water flux through these pores may be much smaller once they are completely filled with water and water can only leave these pores by infiltrating into the soil matrix. Therefore, using the measured saturated hydraulic conductivity on short soil columns together with the Mualem model and a unimodal pore size distribution model (van Genuchten water retention curve) may lead to a strong overestimation of the unsaturated hydraulic conductivity of structured soils (e.g., Schaap and Leij, 2000; Weynants et al., 2009). The retrieved parameters were derived by fitting the coupled model to time series of brightness temperatures, and the corresponding moisture contents represented most of the times with unsaturated soil conditions. As a consequence, the retrieved parameters represent the hydraulic properties under unsaturated conditions. Because of the impact of interaggregate pores on the measured saturated hydraulic conductivity and on the retrieved saturated water content, which was larger than the saturated water content measured in the laboratory, the retrieved hydraulic conductivity for a given water content was considerably lower than the hydraulic conductivity that was derived from the laboratory parameters. The bimodal pore size distribution model has the flexibility to represent the impact of interaggregate pores or macropores on the hydraulic properties. It should be noted that for all except the dry period (DOY 92–120, 2011), the DBM model predicted higher hydraulic conductivities close to saturation, i.e., for $h > -1$ cm, than the MvG model. whereas for lower pressure heads, i.e., $h < -10$ cm, the hydraulic conductivities obtained with the DBM model were generally smaller than those derived using the MvG model (see Fig. 7).

Site- and Depth-Specific Calibration of Soil Moisture Sensors

The relationship between the relative dielectric permittivity ε_r obtained from the 5TE sensors and the corresponding volumetric soil moisture is presented in Fig. 8 for two sensor depths: 2 and 5 cm. For sensors that were installed deeper in the calibration box, the relationship did not differ substantially from the sensor at the 5-cm depth (results not shown), as was expected because the soil was uniformly packed in the box, the water content did not vary with depth, and the measurement volume of the deeper sensors

was completely within the calibration box and did not include an additional air layer. The data points were fitted by a quadratic relationship, which was found also appropriate for other soil types (Cobos and Chambers, 2011), using a least squares method. Also shown in Fig. 8 is the Topp equation (Topp et al., 1980), which is used by the software provided by the manufacturer to convert the measured dielectric permittivity to volumetric soil moisture.

The relation between sensor-derived dielectric permittivity and water content was clearly different for the sensors installed at the 2- and 5-cm depths. For the same soil water content, the dielectric permittivity that was derived by the sensor at the 2-cm depth was lower than the dielectric permittivity derived from the sensor at the 5-cm depth. This is consistent with the anticipated effect of the low dielectric permittivity of the air layer above the soil surface on the dielectric permittivity measured by a sensor installed close to the soil surface. The implication of this different relationship for 5TE sensors installed at the 2-cm depth can be an underestimation of the soil moisture content of up to 0.05 cm^3 cm^{-3} when a relationship for sensors that are installed deeper is used.

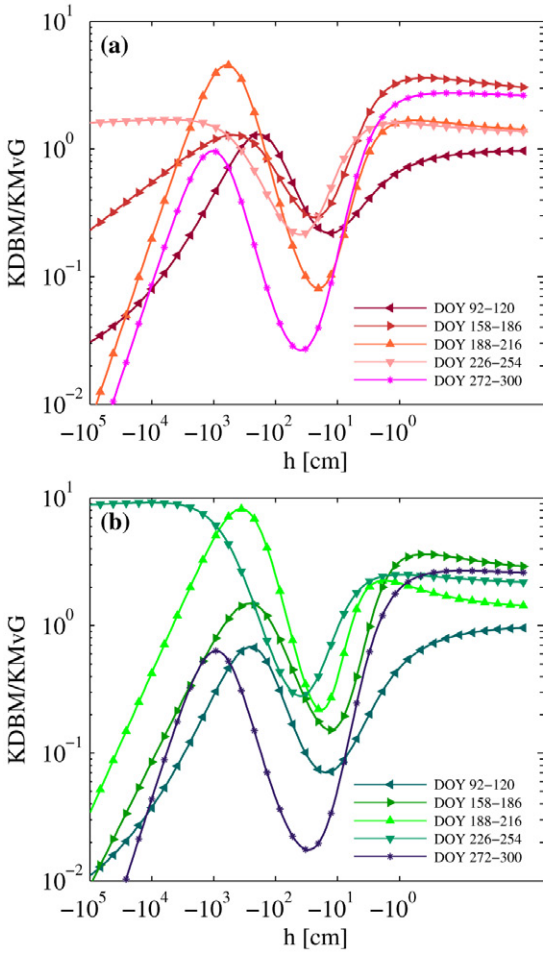

Fig. 7. Ratio of the Durner bimodal to the Mualem–van Genuchten unsaturated hydraulic conductivities (KDBM/KMvG) as a function of pressure head, *h*, which were retrieved for the different time periods (in Day of the Year, DOY) from brightness temperatures using (a) the coherent radiative transfer model or (b) the Fresnel equation.

The relation between sensor-derived dielectric permittivity and soil moisture content also deviated considerably from the Topp equation. This deviation (e.g., for $\varepsilon_r = 15$, the deviation is >0.1 cm^3 cm^{-3}) was found to be considerably larger than the accuracy of the soil moisture measurement that is suggested by the manufacturer to be $\pm$ 0.03 cm^3 cm^{-3}. We do not understand well the causes for this deviation but it should be noted that this deviation does not necessarily imply that Topp's equation is not valid for this soil. It could also indicate that the sensor-derived dielectric permittivity deviates from the bulk soil dielectric permittivity due to disturbances of the soil close to the sensor, such as air gaps or local soil compaction around the sensor.

Comparison between Retrieved and In Situ Measured Soil Moisture Contents

Figure 9 shows measured and retrieved soil moisture using the DBM in combination with the CRTM, Fresnel 0–2 cm, or Fresnel 0–5 cm models at the 2- and 5-cm depths for the two considered observation periods. Similar figures for other time periods are given in the supplementary material (Supplementary Fig. A3 and A4). Overall, a good agreement between retrieved and measured soil moisture contents was obtained. However, the changes in retrieved and sensor-measured water contents after a rainfall event differed considerably. After main rain events, the measured TBH values decreased by >50 K (e.g., at DOY 93, 102.5, and 117.41, as well as DOY 162.6, 167.6, and 180, see Fig. 4). The maximum changes in the measured soil water content values after rain events were 0.04 cm^3 cm^{-3} at 2 cm and 0.024 cm^3 cm^{-3} at 5 cm for the dry period and 0.07 cm^3 cm^{-3} at 2 cm and 0.056 cm^3 cm^{-3} at 5 cm for the wet period. The maximum changes in the retrieved soil

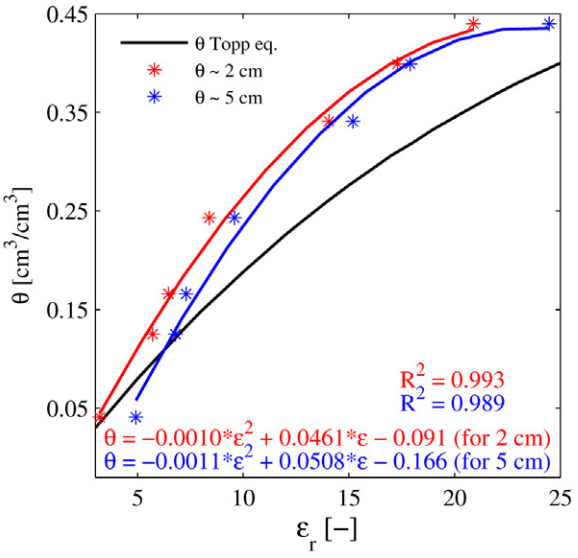

Fig. 8. Relation between gravimetrically measured volumetric moisture content, θ, and relative dielectric permittivity, ε_r, measured by Decagon 5TE sensors at 2 and 5 cm below the soil surface. The colored lines are fits of a quadratic equation through the measurement points and the black line represents the Topp equation (Topp et al., 1980), which is used by the sensors to calculate soil moisture.

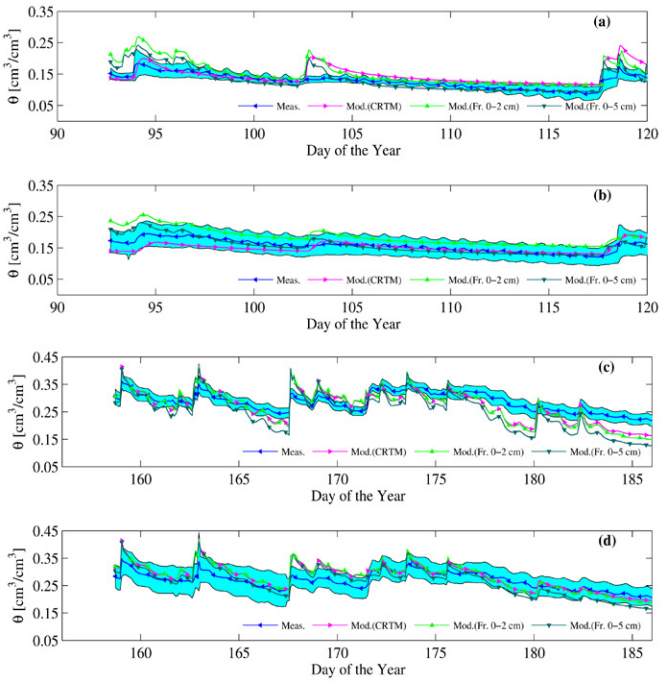

Fig. 9. Time series for (a,b) Day of the Year (DOY) 92 to 120, 2011, and (c,d) DOY 158 to 186, 2011, and (a,c) 2-cm and (b,d) 5-cm depths of volumetric soil moisture contents, θ, that were obtained from sensor readings using a site- and depth-specific calibration (blue lines) and retrieved from L-band brightness temperatures using the Durner bimodal hydraulic model coupled with the coherent radiative transfer model (CRTM) or with the Fresnel equation (Fr.) using the mean dielectric permittivity of the 0- to 2- or 0- to 5-cm layer. The transparent blue bands around the sensor readings represent the 95% confidence intervals of the mean of the sensor readings at a certain time and depth.

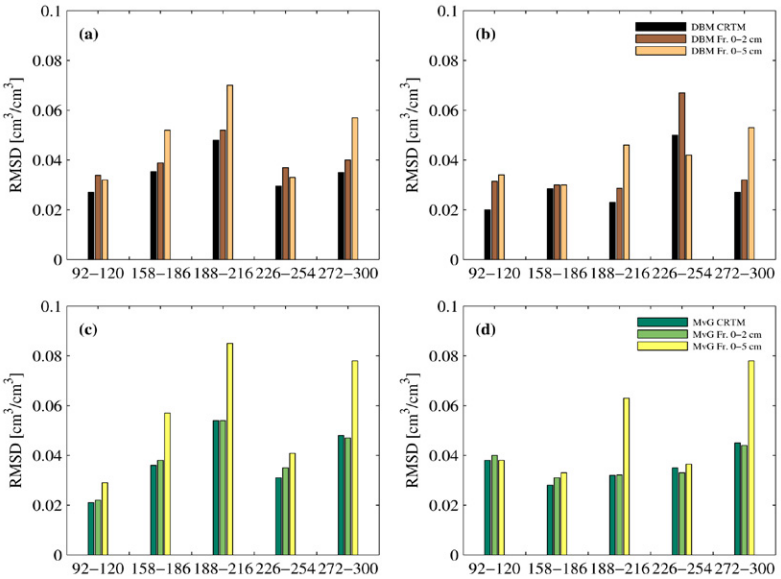

Fig. 10. Root mean square deviations (RMSDs) between measured soil moisture contents using a site- and depth-specific calibration and retrieved soil moisture contents at (a,c) 2-cm and (b,d) 5-cm depths for all investigated periods (*x* axis in Day of the Year) and for different combinations of radiative transfer models: coherent radiative transfer model (CRTM) or the Fresnel equation (Fr.) with depth-averaged dielectric permittivity in the 0- to 2- or 0- to 5-cm surface layer and different soil hydraulic functions: (a,b) Durner bimodal model (DBM) or (c,d) Mualem–van Genuchten (MvG).

water content values using CRTM after rain events were considerably larger than the changes measured by the soil sensors. The retrieved soil moisture changes were 0.14 $cm^3\ cm^{-3}$ at 2 cm and 0.009 $cm^3\ cm^{-3}$ at 5 cm for the dry period and 0.21 $cm^3\ cm^{-3}$ at 2 cm and 0.12 $cm^3\ cm^{-3}$ at 5 cm for the wet period.

The soil hydrologic model simulates with high vertical resolution the temporal changes in water content and consequently dielectric permittivity distributions within the topsoil layer during and after a rainfall event, and their impact on the brightness temperature is modeled using the CRTM radiative transfer model. This implies that the difference in dynamics of retrieved and sensor-measured soil moisture contents after a rainfall event cannot be attributed to neglecting vertical variations in soil moisture and dielectric permittivity in the topsoil layer in the retrieval algorithm.

In Fig. 10a and 10d, the RMSDs between the in situ measured soil moisture using the depth- and site-specific calibration and moisture contents retrieved from brightness temperatures using different radiative transfer models (CRTM, Fresnel 0–2 cm, and Fresnel 0–5 cm) and different soil hydraulic functions (DBM and MvG) are shown. The RMSD values with CRTM were, for both soil hydraulic properties models—DBM and MvG—mostly slightly lower than the values obtained with Fresnel 0–2 cm and Fresnel 0–5 cm (except for the dry period DOY 92–120, 2011, at 2 cm). However, the RMSD values estimated with Fresnel 0–5 cm were always higher than the other two (except wet period DOY 226–254, 2011, where all values were identical). The similar RMSDs between observed and retrieved soil moisture contents for the CRTM and Fresnel 0–2 cm suggested that simulated vertical variations in soil water content in the upper 2-cm soil layer were not so important for the brightness temperatures.

Figure 11 shows the retrieved water contents when the MvG or the DBM hydraulic functions are used together with the CRTM radiative transfer model. When comparing the RMSDs obtained for the DBM and MvG hydraulic functions (see Fig. 10), the DBM leads in general to smaller RMSDs than the MvG. The smaller RMSDs between observed and simulated brightness temperatures for the CRTM and DBM model combination (Fig. 5) were apparently transferred into smaller RMSDs between retrieved and measured soil moisture contents. However, it must be noted that the effects were small and not always present.

In the previous comparisons, sensor-measured water contents were compared with simulated water contents at a given depth. To evaluate the effect on this comparison of vertical averaging of water contents by soil sensors, depth-weighted averages of the retrieved soil moisture contents were compared with the retrieved

soil moisture contents at a single depth (2- and 5-cm depths) and plotted together in Fig. 12. For 5 cm, the depth-averaged retrieved water contents were very similar to those retrieved at 5 cm. For the 2-cm depth, the vertically averaged retrieved soil moisture contents, which include low water contents in an air layer above the soil surface, represent soil moisture contents that would be measured by a sensor installed at the 2-cm depth when no depth-specific calibration would be used. Excluding the air layer from the calculation of depth-averaged moisture contents (i.e., by dividing the depth-weighted averaged water content in the 0- to 5.25-cm layer by the integral of weighting factors in this layer) considerably reduced the difference between the depth-averaged moisture contents and the moisture contents at 2 cm. This indicates that the moisture content that would be derived from a sensor installed at the 2-cm depth using a depth-specific calibration is not very different from the soil moisture at the 2-cm depth. It must be noted that the vertical averaging and the thickness of the air layer that was considered in this averaging procedure was based on a very crude assessment.

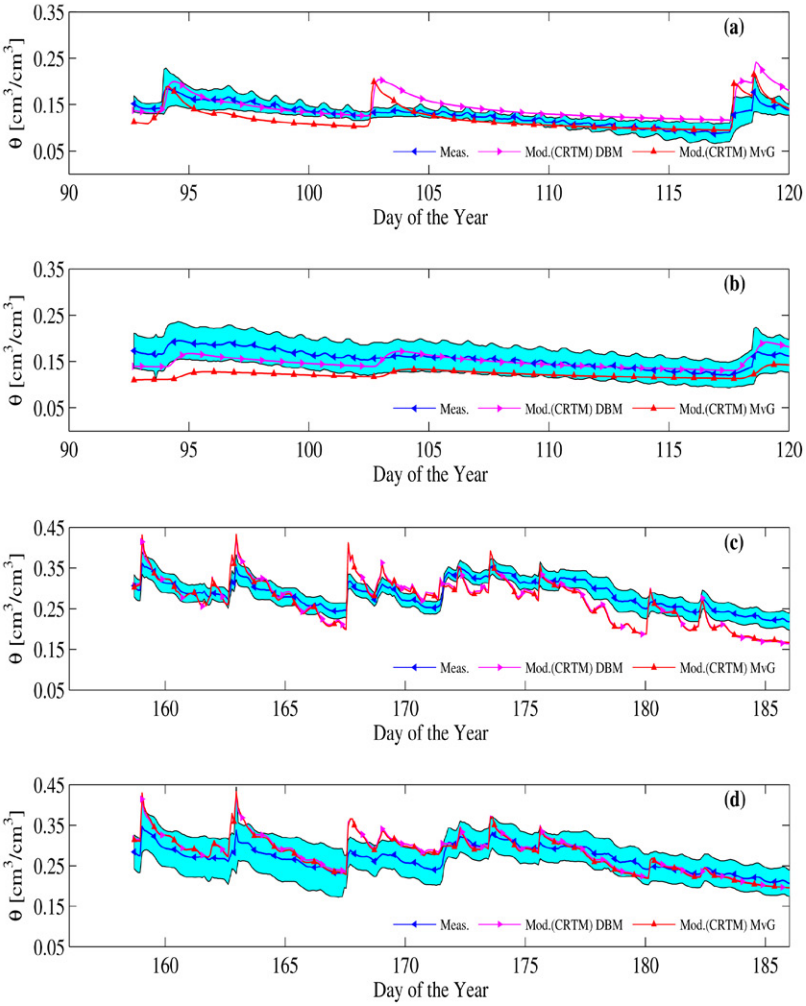

Fig. 11. Time series for (a,b) Day of the Year (DOY) 92 to 120, 2011, and (c,d) DOY 158 to 186, 2011, and (a,c) 2-cm and (b,d) 5-cm depths of volumetric soil moisture contents, θ, that were obtained from sensor readings using a site- and depth-specific calibration (blue lines) and retrieved from brightness temperatures using the coherent radiative transfer model (CRTM) and the Durner bimodal or the Mualem van Genuchten model. The transparent blue bands represent the 95% confidence intervals of the mean of measured moisture contents at a certain time and depth.

Summary and Conclusions

We monitored L-band brightness temperatures at horizontal polarization (TBH) of a tilled bare soil plot with a relatively high surface roughness. This was done for five 28-d periods so as to cover the range of soil hydrologic conditions that may occur in different seasons of a temperate humid climate. From the measured brightness temperatures and the meteorological conditions at the site, soil surface roughness and soil hydraulic parameters were estimated using a closed-loop inversion that linked a soil hydrologic model with a roughness correction model and a radiative transfer model. The different 28-d periods were independently inverted so that the variation and consistency of the inverted parameters with independent measurements could be assessed. For the hydrologic model, two models that describe the soil hydraulic properties were considered: the unimodal MvG and the DBM. For radiative transfer, a CRTM that accounts for the effect of vertical variations in dielectric permittivity and the Fresnel model that predicts the emission from a soil profile with a vertically uniform dielectric permittivity, which was taken to be the average soil permittivity of a soil layer between 0 and 2 or between 0 and 5 cm, were considered. The CRTM model in combination with the DBM model offered the most flexibility to match the simulated and measured TBHs (RMSDs between 4.4 and 12.3 K in the different periods). The results with Fresnel 0–2 cm were better than the results with Fresnel 0–5 cm and similar to the results obtained with the CRTM. Based on this, it might be concluded that for this soil, a Fresnel model with a 2-cm layer thickness may be used to describe the brightness temperature dynamics.

A second important aspect of this study was the validation of the retrieved parameters, in our case soil surface roughness and soil hydraulic properties, and the validation of the retrieved soil moisture contents by in situ measurements. The estimated values of the roughness parameter compared well with the observations made with the laser profiler, except for the dry period (DOY 92–120) when the model overestimated the roughness parameter. Considering the semi-empirical nature of the surface roughness correction model and the spatial and temporal variability of soil surface roughness during the investigated periods, however, it seems difficult to obtain better correspondence.

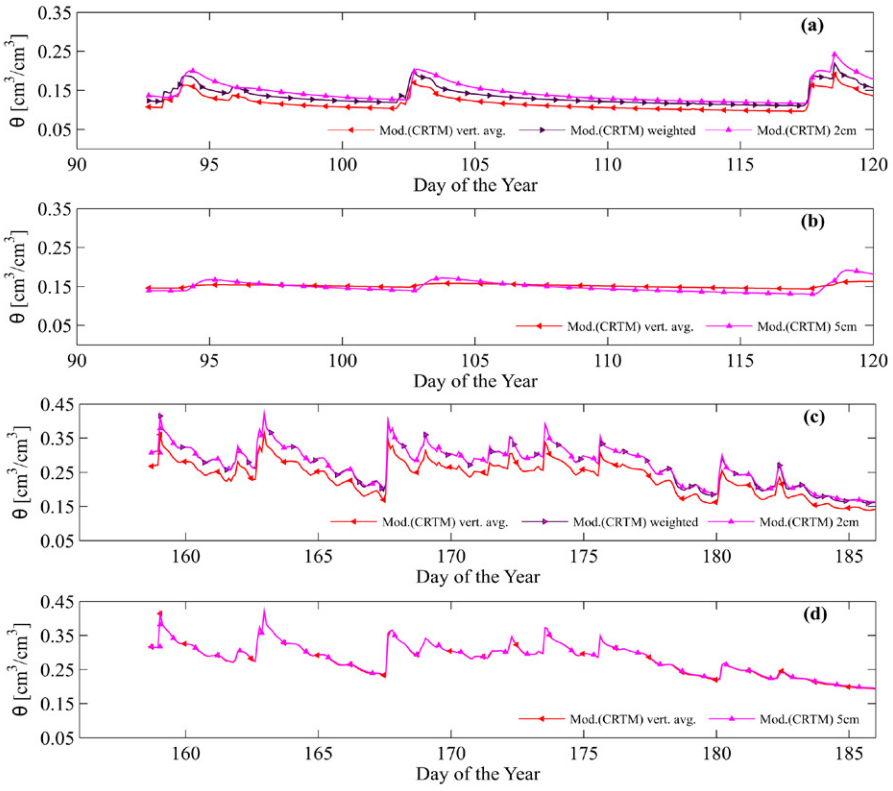

Fig. 12. Time series for (a,b) Day of the Year (DOY) 92 to 120, 2011, and (c,d) DOY 158 to 186, 2011, and (a,c) 2-cm and (b,d) 5-cm depths of volumetric soil moisture contents, θ, that were retrieved from brightness temperatures using the coherent radiative transfer model (CRTM) and the Durner bimodal model: at the respective depths; averaged across the entire presumed sensor's measurement volume, i.e., with inclusion of an air layer for the sensor installed at the 2-cm depth (vert. avg.); or averaged across the sensor's measurement volume excluding this air layer (weighted).

The retrieved soil hydraulic properties were compared with soil hydraulic properties measured on soil columns in the laboratory. Despite the fact that soil surface was homogenized by tillage, the hydraulic properties of the different soil cores varied considerably, which may be attributed to their relatively small size (100 cm^3). Furthermore, the difference in spatial scale of the footprint of the radiometer and the soil columns may also have resulted in differences between retrieved and directly measured soil hydraulic properties. The measured water retention curves from the soil cores indicated a bimodal pore size distribution, which justified the use of the DBM model for the inversion of the brightness temperatures. The retrieved retention curves for the different periods varied, but all showed similar bimodal distributions. This indicates that the time courses of the brightness temperatures contain some information about the multimodal shape of the water retention curve. A comparison between measured and retrieved unsaturated hydraulic conductivity curves is more difficult because no measurements containing information about the unsaturated hydraulic conductivity were done in the laboratory. When comparing the measured with retrieved saturated hydraulic conductivities, the retrieved saturated conductivities for the MvG model were smaller than the measured ones. This can be explained by the drastic change in the hydraulic conductivity close to saturation, which is typical for well-structured soils with a well-developed interaggregate pore network besides the micropore network. The MvG model, which represents only one pore size distribution, tries to find a compromise between the high conductivities close to saturation and the lower conductivities under unsaturated conditions. The DBM model has more flexibility and the retrieved DBM conductivity curves showed a higher conductivity close to saturation and lower conductivity for more negative pressure heads than the MvG.

Finally, the retrieved soil moisture contents were compared with in situ measurements. Similar to the brightness temperatures, we found that soil moisture contents that were retrieved using the CRTM model or Fresnel 0–2 cm model corresponded better with the in situ measured moisture contents than the retrieved moisture contents using the Fresnel 0–5 cm model. This indicates that brightness temperatures are sensitive to soil moisture contents near the soil surface.

However, measuring soil moisture using in situ sensors close to the soil surface is a challenge. Only when a depth- and site-specific calibration relation was used did the retrieved and measured soil moisture contents compare relatively well. The RMSDs between measured and retrieved soil moisture contents were slightly lower for the DBM than for the MvG model. The better fit of the brightness temperatures by the DBM model is therefore also translated into a better description of the soil moisture. However, the dynamics of the retrieved soil moisture, i.e., the change in water content just after a rain event, did not agree with that measured by the soil moisture sensors. It remains an open question whether this was due to a problem with the soil moisture sensors or the radiative transfer models for rough soil surfaces.

Acknowledgments

This study is a part of the research unit FOR 1083 MUSIS (Multi-Scale Interfaces in Unsaturated Soil) funded by the German Research Foundation (DFG). We thank Prof. Dr. P.-S. Lammers and Dr. Lutz Damerow (Institute of Agriculture Engineering) for providing the laser profiler. We thank the team of H. Jagdfeld (Central Institute of Technology, Research Centre Jülich) for the development of the holding construction of the radiometer; the team of A. Egmen and D. Schnabel (technician workshop of IBG, Research Centre Jülich) for building the holding construction of the radiometer. We thank C. Steenpass, Dr. U. Rosenbaum, and Dr. F. Jonard for support during the development of the inversion approach. We thank the technician staff of the Agrosphere Institute, especially R. Harms and F. Engels, for technical support during the measurements; A. Langen for laboratory measurements of the soil hydraulic properties, and N. Hermes for the logging software for the radiometer data. M. Dimitrov thanks Dr. S. Huisman, Dr. A. Graf, Dr. J. Bikowski, Dr. I. Mladenova and Dr. Th. Holmes for all of the consultations and the model improvement. The USDA is an equal opportunity provider and employer.

References

Allen, R.G., L.S. Pereira, D. Raes, and M. Smith. 1998. Crop evapotranspiration (guidelines for computing crop water requirements). Irrig. Drain. Pap. 56. FAO, Rome.

Bass, M., E.W. Van Stryland, D.R. Williams, and W.L. Wolfe. 1995. Optical properties of films and coatings. In: M. Bass, editor, Handbook of optics. Vol. I. McGraw-Hill, New York. p. 42.9–42.14.

Bindlish, R., T.J. Jackson, A. Gasiewski, B. Stankov, M. Klein, M.H. Cosh, et al. 2008. Aircraft based soil moisture retrievals under mixed vegetation and topographic conditions. Remote Sens. Environ. 112:375–390. doi:10.1016/j.rse.2007.01.024

Burke, E.J., R.J. Gurney, L.P. Simmonds, and P.E. O'Neill. 1998. Using a modeling approach to predict soil hydraulic properties from passive microwave measurements. IEEE Trans. Geosci. Remote Sens. 36:454–462. doi:10.1109/36.662729

Camillo, P.J., P.E. O'Neill, and R.J. Gurney. 1986. Estimating soil hydraulic parameters using passive microwave data. IEEE Trans. Geosci. Remote Sens. 24:930–936. doi:10.1109/TGRS.1986.289708

Chang, D.-H., and S. Islam. 2000. Estimation of soil physical properties using remote sensing and artificial neural network. Remote Sens. Environ. 74:534–544. doi:10.1016/S0034-4257(00)00144-9

Chanzy, A., M. Mumen, and G. Richard. 2008. Accuracy of top soil moisture simulation using a mechanistic model with limited soil characterization. Water Resour. Res. 44:W03432. doi:10.1029/2006WR005765

Choudhury, B.J., T.J. Schmugge, A. Chang, and R.W. Newton. 1979. Effect of surface roughness on the microwave emission from soils. J. Geophys. Res.: Oceans 84:5699–5706. doi:10.1029/JC084iC09p05699

Choudhury, B.J., T. Schmugge, and T. Mo. 1982. A parameterization of effective soil temperature for microwave emission. J. Geophys. Res.: Oceans 87:1301–1304. doi:10.1029/JC087iC02p01301

Cobos, D.R., and C. Chambers. 2011. Calibrating ECH$_2$O soil moisture sensors. Appl. Note. Decagon Devices, Pullman, WA.

Decagon Devices. 2009. Frequently asked questions about Decagon's soil moisture probes and accessories. Appl. Note. Decagon Devices, Pullman, WA.

Decagon Devices. 2010. 5TE, water content, EC and temperature sensors: Operator's manual, version 6. Decagon Devices, Pullman, WA.

de Rosnay, P., J.-C. Calvet, Y. Kerr, J.-P. Wigneron, F. Lemaître, M. J. Escorihuela, et al. 2006. SMOSREX: A long term field campaign experiment for soil moisture and land surface processes remote sensing. Remote Sens. Environ. 102:377–389. doi:10.1016/j.rse.2006.02.021

Duan, Q., V.K. Gupta, and S. Sorooshian. 1993. Shuffled complex evolution approach for effective and efficient global minimization. J. Optim. Theory Appl. 76:501–521. doi:10.1007/BF00939380

Durner, W. 1994. Hydraulic conductivity estimation for soils with heterogeneous pore structure. Water Resour. Res. 30:211–223. doi:10.1029/93WR02676

Entekhabi, D., E.G. Njoku, P.E. O'Neill, K.H. Kellogg, W.T. Crow, W.N. Edelstein, et al. 2010. The Soil Moisture Active Passive (SMAP) mission. Proc. IEEE 98:704–716.

Escorihuela, M., J.A. Chanzy, J.P. Wigneron, and Y.H. Kerr. 2010. Effective soil moisture sampling depth of L-band radiometry: A case study. Remote Sens. Environ. 114:995–1001. doi:10.1016/j.rse.2009.12.011

Fung, A.K. 1994. Microwave scattering and emission models and their application. Artech House, Norwood, MA.

Holmes, T.R.H., P. de Rosnay, R. de Jeu, J.-P. Wigneron, Y. Kerr, J.-C. Calvet, et al. 2006. A new parameterization of the effective temperature for L-band radiometry. Geophys. Res. Lett. 33:L07405. doi:10.1029/2006GL025724

Jackson, T.J., D.M. Le Vine, A.Y. Hsu, A. Oldak, P.J. Starks, C.T. Swift, et al. 1999. Soil moisture mapping at regional scales using microwave radiometry: The Southern Great Plains Hydrology Experiment. IEEE Trans. Geosci. Remote Sens. 37:2136–2151. doi:10.1109/36.789610

Jackson, T.J., P.E. O'Neill, and C.T. Swift. 1997. Passive microwave observation of diurnal surface soil moisture. IEEE Trans. Geosci. Remote Sens. 35:1210–1222. doi:10.1109/36.628788

Jadoon, K.Z., L. Weihermüller, B. Scharnagl, M.B. Kowalsky, M. Bechtold, S.S. Hubbard, et al. 2012. Estimation of field-scale soil hydraulic parameters by integrated hydrogeophysical inversion of time-lapse ground-penetrating radar data. Vadose Zone J. 11(4). doi:10.2136/vzj2011.0177

Jonard, F., L. Weihermüller, K.Z. Jadoon, M. Schwank, H. Vereecken, and S. Lambot. 2011. Mapping field-scale soil moisture with L-band radiometer and ground-penetrating radar over bare soil. IEEE Trans. Geosci. Remote Sens. 49:2863–2875. doi:10.1109/TGRS.2011.2114890

Jury, W.A., W.R. Gardner, and W.H. Gardner. 1996. Soil physics. 5th ed. John Wiley & Sons, New York.

Kerr, Y.H., P. Waldteufel, J.-P. Wigneron, S. Delwart, F. Cabot, J. Boutin, et al. 2010. The SMOS mission: New tool for monitoring key elements of the global water cycle. Proc. IEEE 98:666–687. doi:10.1109/JPROC.2010.2043032

Kostov, K.G., and B.I. Vichev. 1995. Near-surface moisture profile effects on the microwave emission of bare soils. In: T.I. Stein, editor, Proc. IGARSS'95: Quantitative Remote Sensing for Science and Applications, Florence, Italy. 10–14 July 1995. Vol. 3. IEEE, New York. p. 1991–1993.

Lambot, S., E. Slob, J. Rhebergen, O. Lopera, K.Z. Jadoon, and H. Vereecken. 2009. Remote estimation of the hydraulic properties of a sand using full-waveform integrated hydrogeophysical inversion of time-lapse, off-ground GPR data. Vadose Zone J. 8:743–754. doi:10.2136/vzj2008.0058

Mattikalli, N.M., E.T. Engman, L. Ahuja, and T.J. Jackson. 1995. Estimating soil properties from microwave measurements of soil moisture. Proc. SPIE 2585:89–101.

Mattikalli, N.M., E.T. Engman, T.J. Jackson, and L. Ahuja. 1998. Microwave remote sensing of temporal variations of brightness temperature and near-surface soil water content during a watershed-scale field experiment, and its application to the estimation of soil physical properties. Water Resour. Res. 34:2289–2299. doi:10.1029/98WR00553

Mätzler, C., D. Weber, M. Wuthrich, K. Schneeberger, C. Stamm, H. Wydler, and H. Flühler. 2003. ELBARA, the ETH L-band radiometer for soil-moisture research. In: Proc. 23rd IEEE International Geoscience and Remote Sensing Symposium (IGARSS), Toulouse, France. 21–25 July 2003. IEEE, New York. p. 3058–3060.

Montzka, C., H. Bogena, L. Weihermüller, F. Jonard, C. Bouzinac, J. Kainulainen, et al. 2012. Brightness temperature and soil moisture validation at different scales during the SMOS Validation Campaign in the Rur and Erft catchments, Germany. IEEE Trans. Geosci. Remote Sens. 51:1728–1743. doi:10.1109/TGRS.2012.2206031

Mualem, Y. 1976. A new model for predicting the hydraulic conductivity of unsaturated porous media. Water Resour. Res. 12:513–521. doi:10.1029/WR012i003p00513

Newton, R.W., Q.R. Black, S. Makanvand, A.J. Blanchard, and B.R. Jean. 1982. Soil moisture information and thermal microwave emission. IEEE Trans. Geosci. Remote Sens. 20:275–281.

Njoku, E.G., and D. Entekhabi. 1996. Passive microwave remote sensing of soil moisture. J. Hydrol. 184:101–129. doi:10.1016/0022-1694(95)02970-2

Pellarin, T., J.P. Wigneron, J.C. Calvet, M. Berger, H. Douville, P. Ferrazzoli, et al. 2003. Two-year global simulation of L-band brightness temperatures over land. IEEE Trans. Geosci. Rem. Sens. 41:2135–2139. doi:10.1109/TGRS.2003.815417

Priesack, E., and W. Durner. 2006. Closed-form expression for the multimodal unsaturated conductivity function. Vadose Zone J. 5:121–124. doi:10.2136/vzj2005.0066

Robinson, D.A., C.S. Campbell, J.W. Hopmans, B.K. Hornbuckle, S.B. Jones, R. Knight, et al. 2008. Soil moisture measurements for ecological and hydrological watershed scale observatories: A review. Vadose Zone J. 7:358–389. doi:10.2136/vzj2007.0143

Roth, K., R. Schulin, H. Flühler, and W. Attinger. 1990. Calibration of time domain reflectometry for water content measurement using a composite dielectric approach. Water Resour. Res. 26:2267–2273.

Schaap, M.G., and F.J. Leij. 2000. Improved prediction of unsaturated hydraulic conductivity with the Mualem–van Genuchten model. Soil Sci. Soc. Am. J. 64:843–851. doi:10.2136/sssaj2000.643843x

Schmugge, T. 1985. Remote sensing of soil moisture. In: M.G. Anderson and T.B. Burt, editors, Hydrological forecasting. John Wiley & Sons, New York. p. 101–124.

Schwank, M., I. Völksch, J.P. Wigneron, Y. Kerr, A. Mialon, P. de Rosnay, and C. Mätzler. 2010a. Comparison of two bare-soil reflectivity models and validation with L-band radiometer measurements. IEEE Trans. Geosci. Remote Sens. 48:325–337. doi:10.1109/TGRS.2009.2026894

Schwank, M., A. Wiesmann, C. Werner, C. Mätzler, D. Weber, A. Murk, et al. 2010b. ELBARA II, an L-band radiometer system for soil moisture research. Sensors 10:584–612. doi:10.3390/s100100584

Schwank, M., J.-P. Wigneron, E. Lopez-Baeza, I. Völksch, C. Mätzler, and Y. Kerr. 2012. L-Band radiative properties of vine vegetation at the SMOSCal/Val Site MELBEX III. IEEE Trans. Geosci. Remote Sens. 50:1587–1601. doi:10.1109/TGRS.2012.2184126

Shutko, A.M. 1982. Microwave radiometry of lands under natural and artificial moistening. IEEE Trans. Geosci. Remote Sens. 20:18–26. doi:10.1109/TGRS.1982.4307514

Šimůnek, J., M. Sejna, H. Saito, M. Sakai, and M.Th. van Genuchten. 2008. The HYDRUS-1D software package for simulating the movement of water, heat, and multiple solutes in variably saturated media. Version 4.08. HYDRUS Softw. Ser. 3. Dep. of Environ. Sci., Univ. of California, Riverside.

Sun, Y., J. Lin, P.S. Lammers, and L. Damerow. 2006. Estimating surface porosity by roughness measurement in a silt-loam field. J. Plant Nutr. Soil Sci. 169:630–632. doi:10.1002/jpln.200521935

Topp, G.C., J.L. Davis, and A.P. Annan. 1980. Electromagnetic determination of soil water content: Measurements in coaxial transmission lines. Water Resour. Res. 16:574–582. doi:10.1029/WR016i003p00574

Ulaby, F.T., R.K. Moore, and A.K. Fung. 1981. Microwave remote sensing: Active and passive. Vol. I. Artech House, Norwood, MA.

Ulaby, F.T., R. Moore, and A.K. Fung. 1982. Microwave remote sensing: Active and passive. Vol. II. Radar remote sensing and surface scattering and emission theory. Artech House, Norwood, MA.

Ulaby, F.T., R.K. Moore, and A.K. Fung. 1986. Microwave remote sensing: Active and passive. Vol. III. From theory to applications. Artech House, Norwood, MA.

van Genuchten, M.Th. 1980. A closed-form equation for predicting the hydraulic conductivity of unsaturated soils. Soil Sci. Soc. Am. J. 44:892–898. doi:10.2136/sssaj1980.03615995004400050002x

Vereecken, H., J.A. Husiman, H. Bogena, J. Vanderborght, J.A. Vrugt, and J.W. Hopmans. 2008. On the value of soil moisture measurements in vadose zone hydrology: A review. Water Resour. Res. 44:W00D06. doi:10.1029/2008WR006829

Vereecken, H., R. Kasteel, J. Vanderborght, and T. Harter. 2007. Upscaling hydraulic properties and soil water flow processes in heterogeneous soils: A review. Vadose Zone J. 6:1–28. doi:10.2136/vzj2006.0055

Wang, J.R. 1987. Microwave emission from smooth bare fields and soil moisture sampling depth. IEEE Trans. Geosci. Remote Sens. 25:616–622. doi:10.1109/TGRS.1987.289840

Wang, J.R., and Th. Schmugge. 1980. An empirical model for the complex dielectric permittivity of soils as a function of water content. IEEE Trans. Geosci. Remote Sens. 18:288–295.

Weihermüller, L., J.A. Huisman, S. Lambot, M. Herbst, and H. Vereecken. 2007. Mapping the spatial variation of soil water content at the field scale with different ground penetrating radar techniques. J. Hydrol. 340:205–216. doi:10.1016/j.jhydrol.2007.04.013

Weynants, M., H. Vereecken, and M. Javaux. 2009. Revisiting Vereecken pedotransfer functions: Introducing a closed-form hydraulic model. Vadose Zone J. 8:86–95. doi:10.2136/vzj2008.0062

Wigneron, J.-P., A. Chanzy, P. de Rosnay, C. Rüdiger, and J.-C. Calvet. 2008. Estimating the effective soil temperature at L-band as a function of soil properties. IEEE Trans. Geosci. Remote Sens. 46:797–807. doi:10.1109/TGRS.2007.914806

Wigneron, J.P., A. Chanzy, Y.H. Kerr, H. Lawrence, J. Shi, M.J. Escorihuela, et al. 2011. Evaluating an improved parameterization of the soil emission in L-MEB. IEEE Trans. Geosci. Remote Sens. 49:1177–1189. doi:10.1109/TGRS.2010.2075935

Wigneron, J.-P., L. Laguerre, and Y. Kerr. 2001. A simple parameterization of the L-band microwave emission from rough agricultural soils. IEEE Trans. Geosci. Remote Sens. 39:1697–1707. doi:10.1109/36.942548

Zacharias, S., H. Bogena, L. Samaniego, M. Mauder, R. Fuß, T. Pütz, et al. 2011. A Network of terrestrial environmental observatories in Germany. Vadose Zone J. 10:955–973. doi:10.2136/vzj2010.0139

Zobeck, T.M., and C.A. Onstand. 1987. Tillage and rainfall effects on random roughness: A review. Soil Tillage Res. 9:1–20. doi:10.1016/0167-1987(87)90047-X